

Strain effects on the magnetic anisotropy of $Y_2Fe_{14}B$ examined by first-principles calculations

Zahra Torbatian,^{1,a)} Taisuke Ozaki,^{2,b)} Shinji Tsuneyuki,^{1,3} and Yoshihiro Gohda^{1,4,c)}

¹Department of Physics, The University of Tokyo, Tokyo 113-0033, Japan

²Research Center for Simulation Science, Japan Advanced Institute of Science and Technology, Nomi 923-1292, Japan

³Institute for Solid State Physics, The University of Tokyo, Kashiwa 277-8581, Japan

⁴Department of Materials Science and Engineering, Tokyo Institute of Technology, Yokohama 226-8502, Japan

(Received 5 January 2014; accepted 4 June 2014; published online 16 June 2014)

We investigate strain effects on the magnetic anisotropy energy (MAE) and the magnetic moment of $Y_2Fe_{14}B$ on the basis of density functional theory. We find that the MAE is significantly enhanced upon compression of the lattice. By applying second-order perturbation theory, the coupling among orbitals that is the most significant in enhancing the perpendicular magnetic anisotropy by the compression is identified to be the $3d_{x^2-y^2}^{\downarrow} - 3d_{xy}^{\downarrow}$ coupling at the Fe j_2 site, thereby we emphasize importance of both the effect of the local density of states and the orbital couplings. © 2014 Author(s). All article content, except where otherwise noted, is licensed under a Creative Commons Attribution 3.0 Unported License. [<http://dx.doi.org/10.1063/1.4883840>]

Strain effects on the magnetic properties of sintered-magnet main phases are important, because sintering and post-sinter thermal processes inevitably induce residual strain. Although a few experimental studies have been made on the dependence of strain for intermetallic compounds consisting of a rare-earth element, iron, and boron ($R_2Fe_{14}B$),¹⁻⁴ the present understanding of this issue is far from complete. In particular, the magnetocrystalline anisotropy, which is a key factor for understanding the high coercivity of Nd-Fe-B sintered permanent magnets having $Nd_2Fe_{14}B$ as the main phase,⁵⁻⁷ is not well understood. In contrast with localized $4f$ electrons, which are relatively insensitive to their surrounding environment, $5d$ electrons and Fe $3d$ electrons are typically strongly affected by lattice strain due to their itinerancy. In this sense, $Y_2Fe_{14}B$ is suitable for studying the effects of strain on itinerant d electrons, because Y is a prototypical f^0 example of rare-earth elements. While the previous calculations for $Y_2Fe_{14}B$ have provided insights into magnetic moments and the magnetic anisotropy of unstrained single crystals,⁸⁻¹² strain effects have not been examined from first principles.

In this work, we report a first-principles study of the strain effects for $Y_2Fe_{14}B$. We show that the magnetic anisotropy of $Y_2Fe_{14}B$ comes mostly from Fe d electrons, while the contribution of Y d electrons is considerably smaller. We find the magnetic anisotropy is significantly enhanced upon compression of the lattice. We also clarify the contribution of each Fe site to the magnetic anisotropy by a quantitative approach using second-order perturbation theory, where the coupling at an Fe j_2 site among occupied and unoccupied states of $3d_{x^2-y^2}$ and $3d_{xy}$ components with

the same spin is found to be prominent in enhancing the perpendicular anisotropy, i.e., perpendicular to the (001) plane (c plane). Our method to identify dominant d -orbital couplings should be a practical tool for uncovering insights for the design of microstructures and even compounds for permanent magnets, as well as nanostructures with high magnetocrystalline anisotropy.^{13,14}

The electronic-structure calculations were made within density functional theory using the OpenMX code,¹⁵ in which pseudoatomic-orbital basis sets and norm-conserving pseudopotentials are used. We employed the Perdew–Burke–Ernzerhof (PBE) exchange–correlation functional in the generalized gradient approximation (GGA). Same as $Nd_2Fe_{14}B$, $Y_2Fe_{14}B$ has a tetragonal unit cell with $P4_2/mnm$ space-group symmetry, containing 68 atoms with six crystallographically distinct Fe sites, two Y sites, and one B site.¹⁶⁻¹⁸ In our calculations, the atomic positions are fully relaxed with the criteria for convergence of the total energy and the force acting on atoms of 10^{-6} Hartree and 10^{-5} Hartree/Bohr, respectively. We carefully checked the convergence of the total energy with respect to the number of k points, finding a $9 \times 9 \times 7$ grid to be sufficiently accurate. The magnetic anisotropy energy (MAE) is defined as the change in the total energy by the rotation of the magnetic moment from the c direction to the a direction, i.e., the [100] direction. Unless otherwise stated, the MAE is calculated self-consistently, where the Kohn–Sham Hamiltonian includes the one-body spin–orbit coupling explicitly as a scalar triple product of the electric field, the momentum, and the Pauli matrix. In addition, we employ our approach using perturbation theory, which is compared with self-consistent calculations, to decompose the MAE into contributions from each orbital coupling. In this approach, the following formulae are used to analyze contributions from each atomic site τ as well as couplings among specific atomic orbitals μ and ν : $E_{SO} = \sum_{\tau} E_{SO}^{\tau}$, $E_{SO}^{\tau} = \sum_{\mu\nu} E_{SO}^{\tau\mu\nu}$, and

^{a)}Present address: Department of Physics, Isfahan University of Technology, 84156-83111 Isfahan, Iran.

^{b)}Present address: Institute for Solid State Physics, The University of Tokyo, Kashiwa 277-8581, Japan.

^{c)}Electronic mail: gohda.y.ab@m.titech.ac.jp

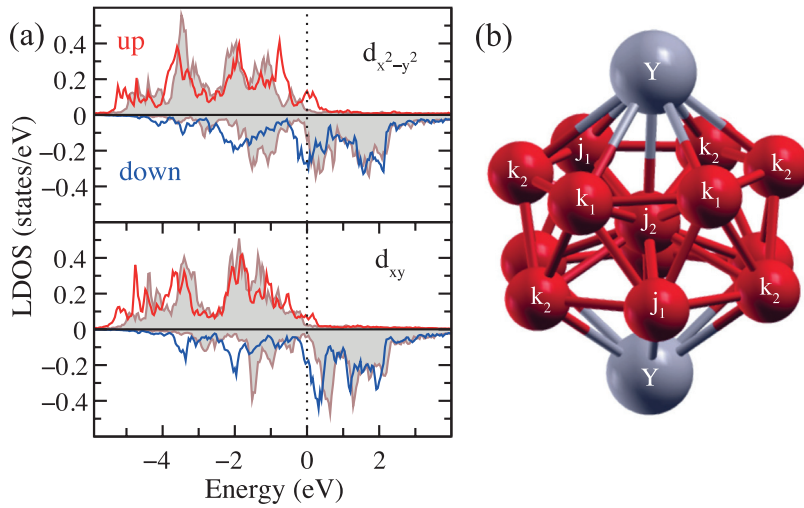


FIG. 1. (a) The LDOS for 3%-compressed $\text{Y}_2\text{Fe}_{14}\text{B}$ at the Fe_{j_2} site projected onto the $3d_{x^2-y^2}$ and $3d_{xy}$ components. The shaded curves are the calculated results in the case without compression. (b) Atomic positions of the NN atoms of the Fe_{j_2} site in $\text{Y}_2\text{Fe}_{14}\text{B}$. The Kohn–Sham eigenenergy ε is referenced to the Fermi energy.

$$E_{\text{SO}}^{\tau\mu\nu} \approx - \sum_i^{\text{occ.}} \sum_j^{\text{unocc.}} \sum_{\tau'\mu'\nu'} \times \frac{\langle i|\tau\mu\rangle \langle \tau\mu|H_{\text{SO}}|\tau\nu\rangle \langle \tau\nu|j\rangle \langle j|\tau'\nu'\rangle \langle \tau'\nu'|H_{\text{SO}}|\tau'\mu'\rangle \langle \tau'\mu'|i\rangle}{\varepsilon_j - \varepsilon_i}, \quad (1)$$

where i and j are occupied and unoccupied Kohn–Sham eigenstates. Note that the indices i , j , μ , and ν include the spin index. In this perturbation scheme, the spin–orbit coupling is approximated as $H_{\text{SO}} = \zeta \mathbf{l} \cdot \mathbf{s}$ considering only on-site contributions of d orbitals. The coupling constants ζ for d electrons are $\zeta_{\text{Fe}} = 62.69$ meV and $\zeta_{\text{Y}} = 41.11$ meV, as obtained by calculations for atoms in Ref. 19. By projecting onto the atomic orbitals μ and ν at a specific atomic site τ , we can use the matrix elements of H_{SO} for each atomic orbital. The matrix elements $\langle \tau\mu|H_{\text{SO}}|\tau\nu\rangle$ for a single atom have been reported for the purpose of qualitative understanding.^{20,21} In contrast, we will use the matrix elements for quantitative identifications of the MAE contributions based on the above formulae, as discussed below. The MAE is calculated by rotating the spins of the Bloch states i and j , whereas the spatial part is kept fixed.

As reported later in detail, we find the magnetic anisotropy of $\text{Y}_2\text{Fe}_{14}\text{B}$ is enhanced upon compression of the lattice. Here, we first describe our most significant findings: By examining all the Fe and Y sites as well as all the possible d -orbital couplings by our perturbation scheme, we have identified that the $d_{x^2-y^2}$ and d_{xy} orbitals at the Fe_{j_2} site play an essential role. Their local density of states (LDOS) and the positions of nearest-neighbor (NN) atoms of the Fe_{j_2} site are shown in Fig. 1. The j_2 site in $\text{Y}_2\text{Fe}_{14}\text{B}$ are sandwiched by double *kagome* layers¹⁶ of Fe having large in-plane interaction, while Y atoms are located nearly along the c axis as seen in Fig. 1(b). This local environment of the j_2 site makes the band widths of $d_{x^2-y^2}$ and d_{xy} more sensitive to the compression than the other orbitals. As a result, both peaks of the $d_{x^2-y^2}^{\uparrow}$ and d_{xy}^{\uparrow} states just above the Fermi energy shift downwards by compression, which results in a significant increase in the LDOS near the Fermi energy.

Since the LDOS is proportional to the absolute square of the coefficients $\langle i|\tau\mu\rangle$ and $\langle \tau\nu|j\rangle$ for the Bloch states i and j in Eq. (1), the high LDOS near the Fermi energy contributes

markedly to the MAE. On the other hand, in considering the matrix element $\langle \tau\mu|H_{\text{SO}}|\tau\nu\rangle$, the coupling between the $d_{x^2-y^2}$ and d_{xy} orbitals, which correspond to angular momenta of $\pm 2\hbar$ in the z direction, with parallel spins makes the largest contribution to the anisotropy in the z direction, as identified by Kyuno *et al.*²⁰ Consequently, combining these two factors, couplings between the occupied (unoccupied) $d_{x^2-y^2}^{\uparrow}$ component and the unoccupied (occupied) d_{xy}^{\downarrow} component, respectively, close to the Fermi energy are explained as the most significant origin of the MAE enhancement upon compression.

Coming back to the unstrained $\text{Y}_2\text{Fe}_{14}\text{B}$ single crystal, the calculated value of the magnetic moment is $31.3 \mu_B/\text{f.u.}$, in excellent agreement with the experimental value of $31.4 \mu_B/\text{f.u.}$ measured at 4.2 K.¹ The electronic states in the vicinity of the Fermi energy are mainly associated with the Fe $3d$ and the Y $4d$ orbitals. The spin polarization of Fe $3d$ bands is much larger than that of Y $4d$ bands. As for the MAE, the magnetic easy axis of $\text{Y}_2\text{Fe}_{14}\text{B}$ is the c axis and this result qualitatively agrees with experiments, even though the calculated value, 0.45 MJ/m^3 , underestimates the experimental one (0.77 MJ/m^3 at 4.2 K (Ref. 6)). This discrepancy in the MAE has been understood as being due to a limitation of the present first-principles methods. It should be noted that the antiferromagnetic coupling among Fe $3d$ and Nd $5d$ orbitals plays a crucial role in the appearance of strong magnetic anisotropy in $\text{Nd}_2\text{Fe}_{14}\text{B}$ (4.3 MJ/m^3 at room temperature⁶). The strong anisotropy of the Nd $4f$ electrons cannot couple with the Fe $3d$ electrons directly, where most of the magnetic moment of the compound comes from.

We now proceed to the lattice-constant dependence of the magnetic moments and the magnetic anisotropy for $\text{Y}_2\text{Fe}_{14}\text{B}$, where the lattice constants, i.e., a and c , are changed by a 3% compression and a 3% expansion independently. Figure 2 shows the behavior of the MAE and magnetic moments with respect to the variation in the lattice constants. The MAE is significantly enhanced upon compression of the lattice, while the magnetic moment decreases. By the compression of both a and c by 3%, the MAE increases from 0.45 MJ/m^3 (2.6 meV/u.c.) to 2.16 MJ/m^3 (11.2 meV/u.c.), while the magnetic moment decreases from $31.3 \mu_B$ to $25.7 \mu_B$. The changes in the MAE and the magnetic moment are much smaller for the expansion. As seen in

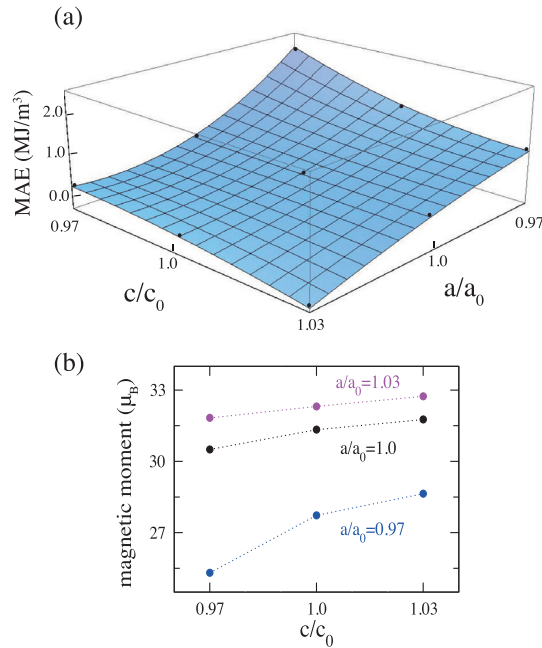


FIG. 2. (a) The MAE and (b) the magnetic moment of $Y_2Fe_{14}B$ as a function of the lattice constants.

Fig. 1(b), the number of NN Fe atoms for the j_2 site is 12. The average of these NN distances changes from 2.67 Å to 2.59 Å upon compression, which is comparable with that for the ferromagnetic fcc Fe theoretically determined as 2.57 Å and is much larger than that for bcc Fe of 2.45 Å. This is consistent with the fact that $R_2Fe_{14}B$ compounds have much lower Curie temperatures compared with bcc Fe.

The DOS of the compressed and expanded $Y_2Fe_{14}B$ are compared with the case for the equilibrium lattice constants in Fig. 3(a). The figure shows that the majority-spin (up-spin) d bands become partially occupied upon compression of the lattice, where the DOS attributable to d electrons becomes broader indicating the enhancement of the electron itinerancy. In contrast, the DOS of the expanded system exhibits slight narrowing of the d -band width attributable to the localization of d electrons. To identify the origin of the strong enhancement of the MAE and the decrease in the magnetic moment, we decompose the total MAE and the magnetic moment into contributions from each atomic site. We decompose the magnetic moment by the LDOS projected

onto Fe atomic orbitals [Fig. 3(b)]. Without strain, the j_2 site has the largest magnetic moment of $2.74 \mu_B$, while the e site exhibits the smallest magnetic moment of $2.13 \mu_B$, as seen in Fig. 3(c). Under the compression, they decrease to $2.54 \mu_B$ and $1.73 \mu_B$, respectively. As Fig. 3(c) shows, the Fe j_1 site has the largest changes under the compression and the expansion. Upon compression, the magnetic moment at the Fe j_1 site decreases considerably from $2.24 \mu_B$ to $1.40 \mu_B$. This drastic decrease in the magnetic moment can be understood from the fact that the up-spin d bands at the j_1 site, which are essentially fully occupied for the case without strain, become partially occupied by the compression-induced modification to the orbital hybridization.²²

In Table I, the total MAE calculated by the perturbation scheme is compared with that by the self-consistent calculations that explicitly include the spin-orbit coupling in the Kohn-Sham Hamiltonian. It is clearly seen that the change in the total MAE by the compression obtained by the self-consistent calculations is reproduced by the perturbation scheme, even though the energy scale is much smaller than the chemical accuracy. The error of the perturbation scheme compared with the self-consistent one is mainly attributed to the on-site approximation with the form of $H_{SO} = \zeta I \cdot s$. In addition, we also compare the perturbation scheme with self-consistent calculations for another intermetallic compound, YFe_3 , in which the MAE obtained by the perturbation scheme (-0.65 MJ/m^3) differs only 0.15 MJ/m^3 from the self-consistent MAE, -0.80 MJ/m^3 .

Next, we discuss the MAE of inequivalent Fe sites as well as the f and g sites of Y listed in Table I. We observe that the symmetry of the MAE is lower than that of the atomic structure for $16k_1$, $16k_2$, and $4c$ sites; e.g., among $16k_1$ sites, eight k_1 sites exhibit one value for the site-decomposed MAE, while the other eight k_1 sites exhibit another. Note that the symmetry of the atomic structure remains unchanged with strain. For each case, $E_{SO}^T(x)$ becomes inequivalent, providing two different values, while the original site symmetry is retained in $E_{SO}^T(z)$. For $E_{SO}(x)$, the spins of the Bloch states in the x direction. The symmetry created by a set of vector quantities can be lower than that created by scalar quantities, i.e., the atomic positions in this case. It is clearly seen that the MAE of $Y_2Fe_{14}B$ essentially comes from the Fe sublattice, where the contribution of Y atoms is negligibly small. For the case of the equilibrium lattice constants, the

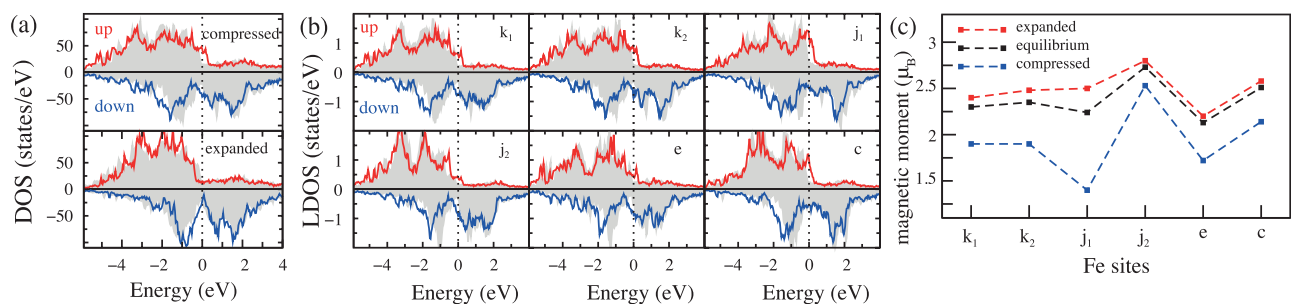


FIG. 3. (a) The DOS for $Y_2Fe_{14}B$ with uniform compression and expansion by 3% in the lattice constants compared with the case for the equilibrium lattice constants (shaded). The single-electron energy is referenced to the Fermi energy. (b) The LDOS of crystallographically inequivalent Fe sites for $Y_2Fe_{14}B$ with the lattice constants compressed uniformly by 3%. The LDOS for the case of the equilibrium lattice constants is shown by shading. (c) Magnetic moment of crystallographically inequivalent Fe sites for $Y_2Fe_{14}B$ with the equilibrium lattice constants and with the lattice constants compressed and expanded uniformly by 3%.

TABLE I. The contribution of the MAE from nine different Fe sites as well as from the f and g sites of Y for $Y_2Fe_{14}B$ with the equilibrium lattice constants and the 3%-compressed lattice constants by the perturbation scheme. The total MAE per unit cell (u.c.) calculated by the present perturbation-theory (PT) scheme is compared with self-consistent (SC) results including spin-orbit coupling non-perturbatively.

$Y_2Fe_{14}B$	Fe sites (meV)								Y sites (meV)		Total MAE (meV)		
	8k ₁	8k ₁	8k ₂	8k ₂	8j ₁	8j ₂	4e	2c	2c	4f	4g	PT	SC
Equilibrium	0.18	-0.08	0.08	0.17	0.23	0.06	0.07	-0.38	-0.42	0.02	0.01	4.0	2.6
Compressed	0.29	0.05	0.27	0.12	0.29	0.58	0.44	-0.15	-0.45	0.02	0.01	13.4	11.2

contribution from the j_1 site is most significant for the perpendicular anisotropy. This fact is consistent with the fact that the LDOS at the Fermi energy for the up spin is among the highest for the j_1 site, as seen in Fig. 3(b). It is also evident that the enhancement of the MAE by the compression comes from that at the Fe j_2 site, where the site-decomposed MAE increases from 0.06 to 0.58 meV. This enhancement of the MAE at the j_2 site is closely related to the increase in the LDOS in the vicinity of the Fermi energy for the down spin shown in Fig. 3(b).

We also analyze the couplings among specific atomic orbitals on the basis of $E_{SO}^{\tau\mu\nu}$. Table II shows the MAE contribution from couplings among the $3d$ orbitals at the j_2 site. We can clearly see that the enhancement of the MAE is related to an increase in the coupling among $d_{x^2-y^2}$ and d_{xy} orbitals from -0.55 to 0.23 meV: The contribution even changes from in-plane anisotropy to perpendicular anisotropy under compression. In more detail, the contribution of $d_{x^2-y^2} - d_{xy}$ coupling at the j_2 site is most significant for the down spins. Under compression, the coupling among $d_{x^2-y^2}^{\downarrow}$ and d_{xy}^{\downarrow} increases from 0.79 meV to 1.43 meV. The other MAE contributions for the compressed system from these d orbitals at the j_2 site are -1.36 meV for $d_{x^2-y^2}^{\downarrow} - d_{xy}^{\downarrow}$, -0.11 meV for $d_{x^2-y^2}^{\uparrow} - d_{xy}^{\uparrow}$, and 0.27 meV for $d_{x^2-y^2}^{\uparrow} - d_{xy}^{\uparrow}$. We also found that couplings among $d_{x^2-y^2}$ and d_{xy} orbitals at the e site have an increase in the MAE upon compression from -0.06 to 0.45 meV, where the coupling among down spins contributes to a MAE change from 0.94 to 1.37 meV.

In summary, we investigated the dependence of the MAE of $Y_2Fe_{14}B$ on the lattice constants by using first-principles calculations. We have found that the magnetic anisotropy of $Y_2Fe_{14}B$ comes from the $3d$ electrons of Fe atoms. The MAE is enhanced by lattice compression. We also proposed a convenient and computationally inexpensive method, based on second-order perturbation theory, to quantify the contribution of each atomic orbital to the MAE. This method quantitatively considers both the effect of the LDOS

TABLE II. The contribution of the MAE of Fe $3d$ orbitals at the j_2 site with the equilibrium lattice constants and the 3%-compressed lattice constants by the present perturbation scheme.

$Y_2Fe_{14}B$	$3d$ orbitals (meV)				
	$d_{x^2-y^2} - d_{xy}$	$d_{yz} - d_{x^2-y^2}$	$d_{z^2} - d_{yz}$	$d_{xz} - d_{yz}$	$d_{xz} - d_{xy}$
Equilibrium	-0.55	0.06	0.48	-0.03	0.10
Compressed	0.23	-0.05	0.37	-0.01	0.05

through matrix elements such as $\langle i|\tau\mu\rangle$ and the effect of orbital couplings $\langle \tau\mu|H_{SO}|\tau\nu\rangle$. With this method, we clarified that the Fe j_2 site makes the highest contribution to the enhanced MAE in the compressed system, where coupling among the $3d_{x^2-y^2}^{\downarrow}$ and $3d_{xy}^{\downarrow}$ orbitals of the j_2 site plays the most significant role. With predictive descriptions of couplings among atomic orbitals for the magnetic anisotropy, our method should be useful for computational designs of permanent-magnet materials utilizing the anisotropy of itinerant d electrons, even without the use of $4f$ electrons of rare-earth elements. On the other hand, it is also interesting to clarify the anisotropy couplings among the Fe sublattice and the $4f$ electrons.

Part of this work has been supported by the Elements Strategy Initiative Center for Magnetic Materials under the outsourcing project of MEXT as well as by Grants-in-Aid for Scientific Research through Contract Nos. 25104705 and 22104006 from MEXT, Japan. The calculations were partly performed on the K-computer (Grant No. hp120086) and supercomputers at ISSP and ITC, The University of Tokyo.

- ¹S. Hirosawa, Y. Matsuura, H. Yamamoto, S. Fujimura, and M. Sagawa, *J. Appl. Phys.* **59**, 873 (1986).
- ²H. Nagata, S. Hirosawa, and M. Sagawa, *J. Magn. Magn. Mater.* **70**, 334 (1987).
- ³M. R. Ibarra, Z. Arnold, P. A. Algarabel, L. Morellon, and J. Kamarad, *J. Phys.: Condens. Matter* **4**, 9721 (1992).
- ⁴V. A. Sidorov and L. G. Khvostantsev, *J. Magn. Magn. Mater.* **129**, 356 (1994).
- ⁵M. Sagawa, S. Fujimura, H. Yamamoto, Y. Matsuura, and S. Hirosawa, *J. Appl. Phys.* **57**, 4094 (1985).
- ⁶S. Hirosawa, Y. Matsuura, H. Yamamoto, S. Fujimura, M. Sagawa, and H. Yamauchi, *Jpn. J. Appl. Phys., Part 2* **24**, L803 (1985).
- ⁷J. M. D. Coey, *IEEE Trans. Magn.* **47**, 4671 (2011).
- ⁸Z.-Q. Gu and W. Y. Ching, *Phys. Rev. B* **33**, 2868 (1986).
- ⁹Z.-Q. Gu and W. Y. Ching, *Phys. Rev. B* **36**, 8530 (1987).
- ¹⁰I. Kitagawa and Y. Asari, *Phys. Rev. B* **81**, 214408 (2010).
- ¹¹M. D. Kuz'min, D. Givord, and V. Skumryev, *J. Appl. Phys.* **107**, 113924 (2010).
- ¹²Y. Miura, H. Tsuchiura, and T. Yoshioka, *J. Appl. Phys.* **115**, 17A765 (2014).
- ¹³K. M. Tsysar, D. I. Bazhanov, E. M. Smelova, and A. M. Saletsky, *Appl. Phys. Lett.* **101**, 043108 (2012).
- ¹⁴A. Thiess, Y. Mokrousov, and S. Heinze, *Phys. Rev. B* **81**, 054433 (2010).
- ¹⁵T. Ozaki, *Phys. Rev. B* **67**, 155108 (2003).
- ¹⁶J. M. D. Coey, *Magnetism and Magnetic Materials* (Cambridge University Press, Cambridge, 2010).
- ¹⁷J. F. Herbst, *Rev. Mod. Phys.* **63**, 819 (1991).
- ¹⁸M. Rosenberg, P. Deppe, and Th. Sinnemann, *Hyperfine Interact.* **45**, 3 (1989).
- ¹⁹Y. Yanase and H. Harima, *Solid State Phys.* **46**, 229 (2011) (in Japanese).
- ²⁰K. Kyuno, J.-G. Ha, R. Yamamoto, and S. Asano, *Jpn. J. Appl. Phys.* **35**, 2774 (1996).
- ²¹F. Gimbert and L. Calmels, *Phys. Rev. B* **86**, 184407 (2012).
- ²²M. Ogura, H. Akai, and J. Kanamori, *J. Phys. Soc. Jpn.* **80**, 104711 (2011).